

phys. stat. sol. **35**, 909 (1969)

Subject classification: 10; 22.5.2

School of Physics, University of New South Wales, Kensington, New South Wales

A Study of Dislocation Arrays at Spherical Indentations in LiF as a Function of Indentation Stress and Strain

By

M. V. SWAIN and B. R. LAWN

A systematic study has been made of the dislocation arrays produced by indenting (001) surfaces of LiF with steel and nylon spheres. The arrays are discussed in terms of position along a curve relating "indentation stress" to "indentation strain", these parameters being determined by the geometry of the contact between indenter and specimen. Three stages of behaviour are distinguished: (i) elastic stage, to which the classical Hertzian contact theory is applicable; (ii) initial yield stage, to which standard yield criteria may be applied to predict the spatial location and critical resolved shear stress for initiation of dislocation motion; (iii) subsequent growth of plastic zone, in which the relative activity of the various slip systems determine the indentation behaviour. A mechanism for the initiation of dislocation flow below an indenting sphere has been proposed on theoretical grounds, and subsequently supported by experimental evidence; this mechanism differs from alternative proposals in that the dislocation sources operate within the interior of the crystal rather than at the crystal surface. An evaluation of the dislocation activation stress for LiF is thereby made, the value obtained being in reasonable agreement with results taken from conventional compression tests. The indentation stress-strain behaviour is then discussed in the light of current thought on indentation theory, and some shortcomings in present ideas are pointed out.

Es wurde eine systematische Untersuchung von Versetzungsanordnungen durchgeführt, die durch Eindrücken von Stahl- und Nylonkugeln auf (001)-Oberflächen von LiF hervorgerufen wurden. Die Anordnungen werden durch Positionsgrößen längs einer Kurve, die die „Eindruckspannung“ mit der „Eindruckdehnung“ verknüpfen, diskutiert. Diese Parameter sind durch die Geometrie des Kontakts zwischen Stempel und Probe bestimmt. Drei Verhaltenszustände werden unterschieden: (1) elastischer Zustand, für den die klassische Hertz'sche Theorie anwendbar ist; (2) Anfangsfließzustand, für den Standardkriterien des Fließens für die Vorhersage der räumlichen Lage und der aufgelösten, kritischen Scherspannung für das Beginnen der Versetzungswanderung angewendet werden können; (3) nachfolgendes Wachsen des plastischen Bereiches, in dem die relativen Aktivitäten der verschiedenen Gleitsysteme das Eindruckverhalten bestimmen. Ein Mechanismus für den Start des Versetzungsfließens unterhalb einer Eindruckkugel wird auf theoretischer Grundlage vorgeschlagen und durch nachfolgende experimentelle Hinweise bestärkt; dieser Mechanismus unterscheidet sich von Alternativvorschlägen dadurch, daß die Versetzungsquellen eher im Inneren des Kristalls als an der Kristalloberfläche wirken. Eine Abschätzung der Versetzungsaktivierungsspannung für LiF wird durchgeführt, der erhaltene Wert befindet sich in befriedigender Übereinstimmung mit den aus konventionellen Kompressionsversuchen erhaltenen Ergebnissen. Das Eindruck-Spannungs-Dehnungsverhalten wird dann im Lichte der laufenden Vorstellungen über die Eindrucktheorie diskutiert und einige Unzulänglichkeiten dieser Ideen werden aufgezeigt.

1. Introduction

The deformation processes involved in the conventional testing of the mechanical properties of solids are usually investigated in terms of a stress-strain curve.

By this means a considerable amount of information concerning the manner in which a given material deforms over a wide range of stress conditions can be systematically tabulated. There is one method of testing, however, in which systematic studies of applied stress as a function of strain have not been extensively made: this is the technique of loading specimens with an indenter of suitably chosen geometry, e.g. a spherical or pointed indenter. Indentation techniques are largely used in routine hardness testing, where the size of a remanent impression left by the indenter may be quickly measured and the indentation pressure thereby evaluated, this giving an index of specimen "hardness". It is only in recent years that researchers have begun to study in some detail, particularly in metals, the deformation patterns surrounding such impressions, and thus to reveal the nature of the physical processes which control the hardness characteristics of a given material. As a result of this activity indentation techniques are becoming more widespread as a valuable tool in their own right for investigating the deformation properties of solids, and in this respect have a number of advantages over the more conventional tests: among these advantages are; simplicity of operation, involving relatively little demand on specimen preparation; ability to perform many tests over a small surface area of a single specimen; possibility of obtaining a measure of physical parameters not obtainable in the more conventional tests; possibility, by virtue of the strongly inhomogeneous nature of the stress field below an indenter, of revealing new types of deformation behaviour.

It is because of this increasing activity in indentation testing that an attempt is made here to characterise the plastic deformation processes that occur in LiF single crystals in terms of "indentation stress" and "indentation strain". For this purpose it is found advantageous to concentrate on spherical rather than pointed indenters for two reasons: firstly, from the standpoint of mathematical tenability the stresses beneath a spherical indenter are more easily specified [1, 2], if only over a restricted range of deformation; secondly, the indentation pressure beneath a spherical indenter can be varied over a wide range, this permitting various phases of the deformation processes to be studied, whereas the indentation pressure remains effectively constant for standard pointed indenters. LiF is chosen as a test material because its plasticity properties have been widely studied, and because it is amenable to studies by optical, etch, and X-ray topographic techniques. Further, while the indentation behaviour of plastically isotropic solids is reasonably well understood [3], comparatively little is known about the parallel behaviour in anisotropic solids; single crystals of LiF provide a particularly good example of the latter class of solid, dislocation glide being confined to a restricted number of crystallographic planes.

2. Indentation Stress-Strain Curve

2.1 Geometric similarity principle

The interpretation of indentation processes is often simplified by making use of the principle of geometric similarity¹), which effectively states that all geometrically similar indents are formed at the same indentation pressure, independent of the size of the indenter [3]. Fig. 1 illustrates the situation for two

¹) Despite its widespread success, this principle is empirical, and must therefore be applied with caution. It fails, for instance, to predict the initiation of Hertzian fractures in brittle solids, in which case the critical indentation pressure depends systematically on the size of the indenter [4].

Fig. 1. Geometric similarity of two spherical indentations. r denotes ball radius, a the radius of the contact circle

spherical indenters: with the materials of the indenter and specimen remaining unchanged for each indentation, it is seen that the displacement field scales with the chordal diameter of contact for geometrically similar indentations. The strain field beneath the two spheres must consequently be identical. Thus, since the size independent ratio a/r determines the geometry of the contact region between sphere and specimen it also determines the strain level, so that a/r may be regarded as a representative "indentation strain". Similarly, since the mean indentation pressure p_0 (indenter load/projected area of indentation) determines the stress level in the specimen, we may regard p_0 as a measure of the "indentation stress". Accordingly, with the strains completely determining the stresses, we have

$$p_0 = f\left(\frac{a}{r}\right). \quad (1)$$

This relation, which is independent of either the mode of deformation beneath the indenter or the anisotropic properties of the specimen, may thereby be regarded as the "indentation stress-strain" characteristic for ball indentations. Its application to the study of fine-grained metals has been discussed at length by Tabor [3].

2.2 Indentation experiments on LiF single crystals

Specimens of LiF, typically $1 \times 1 \times 0.2 \text{ cm}^3$, were prepared by $\{100\}$ cleavage from a large single crystal block (Harshaw crystal). A Kentron microhardness testing machine was then used to make indentation tests on the specimens. An inverted microscope mounted on the crosshead of the testing machine (Fig. 2) permitted the contact between the depressed indenter and the specimen to be observed throughout the indentation procedure. The contact appeared as a central dark spot surrounded by concentric interference rings, the clarity of which depended largely on the nature of the indenter surface. For instance, steel balls gave rise to distinct fringe patterns while nylon balls, with their poorly reflecting surface, gave contacts that could barely be detected. By me-

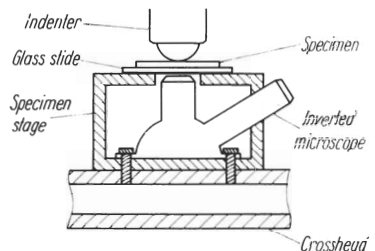
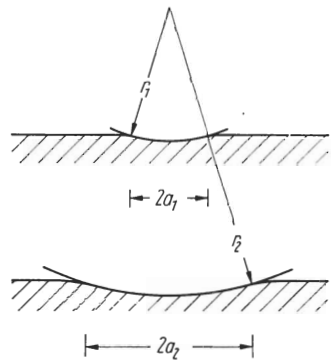


Fig. 2. Experimental arrangement for observing the contact area during an indentation test on a transparent specimen

asuring the spacings of these rings the diameter of contact could be estimated [5].

With the Kentron machine indenter loads within the range $P = 1$ g to 10 kg were possible. Higher loads were obtainable by mounting the indenter into the underside of the cross-head of an Instron testing machine, with the specimen stage seated on a compression load cell. The load rate of the indenters onto the specimen was always kept to a minimum, and contact maintained at the required load for at least one minute.

Indentation tests were thus made on (001) surfaces of LiF using steel balls of diameter $1/2''$, $1/4''$, $1/16''$, and $1/32''$. From the indenter load P , the contact diameter $2a$, and the ball radius r , the mean pressure,

$$p_0 = \frac{P}{\pi a^2}, \quad (2)$$

and the ratio a/r were readily calculable. The resulting stress-strain characteristic (1) for steel spheres is plotted in Fig. 3. Points for the different size steel balls fall onto the one universal curve, thus providing confirmatory evidence for the validity of the geometric similarity principle.

2.3 Compression stress-strain curve of LiF

It will be found instructive in the following sections to compare the curve in Fig. 3 with the stress-strain curve obtained in a standard uniaxial compression test. Specimens of LiF, typically measuring $2 \times 0.6 \times 0.6$ cm³, were cleaved from the same original block as the specimens above. These were lightly etched to remove superfluous surface damage, and were then oriented with their long, [001] axis vertical between two horizontal plattens in an Instron machine. The contact surfaces were lubricated with molybdenum disulphide, and the Instron crosshead driven at 0.01 cm/min. From the load-displacement curve thus obtained the "true" stress-strain curve²⁾ was calculated, assuming the specimen to be incompressible and end-effects to be negligible. A wide variation in behaviour was observed, attributable mainly to frictional end-effects which could

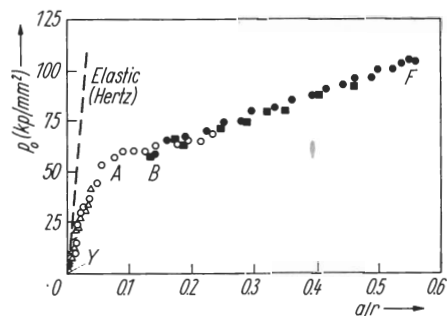


Fig. 3. Indentation stress-strain curve for steel ball indentations on (001) LiF cleavage surfaces. Broken line represents calculated elastic behaviour. Ball diameter: $1/2''$, crosses; $1/4''$, triangles; $1/16''$, circles; $1/32''$, squares. Open symbols denote Kentron data, closed symbols denote Instron data

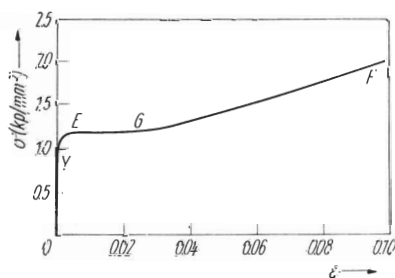


Fig. 4. Compression stress-strain curve for LiF crystals loaded along [001]

²⁾ The "true stress" and "true strain" being defined in terms of the cross-sectional area at a given instant rather than in terms of the original cross-sectional area.

not be completely eliminated, but Fig. 4 represents an average result obtained for a uniformly compressed specimen. This type of stress-strain curve has been well studied [6, 7, 8], and is generally classified in terms of the following stages of deformation: a) elastic region OY; b) initial yield region YE, in which a restricted amount of dislocation motion begins on favourably oriented $\{110\}$ glide planes; c) easy glide region EG, in which glide becomes predominantly active on one set of glide planes only; d) work hardening region GF, in which interactions between the various operative glide systems occur until the specimen fractures.

3. Analysis of Dislocation Arrays on Indented LiF Surfaces

The optical arrangement outlined in Section 2.2 provides a measure of the mutual contact area in an indentation test, but reveals nothing about the dislocation mechanisms by which the specimen deforms. For this latter purpose indentations were examined using mainly etch techniques, with X-ray topography providing useful complementary information. Other standardised optical techniques, two-beam interferometry and stress birefringence, are especially suited to the study of the more severe indentations [9].

With large indentation pressures (say within the range AF of Fig. 3) the deformation around the impressions was gross, resembling the familiar "rosette" patterns on LiF [6]. With small indentation pressures (range OA of Fig. 3) the deformation was less complex but, at the same time, more sensitive to the state of the surfaces of both the indenter and specimen. For instance, the hard asperities on even the most carefully polished steel balls gave rise to a profusion of minor rosettes over the entire area of contact with the specimen. At very low loads this spurious damage precluded the observation of the dislocation arrays created by the genuine Hertzian stresses. Consequently, nylon spheres, with their relatively soft surface irregularities, proved more useful for studying the initial stages of the deformation.

Using the classification scheme for the various deformation stages in the uniaxial compression test as a guide (cf. Section 2.3), an attempt was made to similarly classify the dislocation pattern at spherical indentations in terms of various stages of indentation stress and strain. Despite the apparent resemblance between the curves in Figs. 3 and 4 significant differences were observed in the deformation behaviour, as a result of which it becomes more convenient to discuss the spherical indentation behaviour under the following headings: a) elastic region OY; b) initial dislocation motion at the "yield" point Y; c) plastic zone growth YABF. We discuss each of these stages in turn.

3.1 Elastic stage

Within the elastic range OY of Fig. 3 we may apply the classical Hertzian contact theory [1]. The actual stresses beneath a spherical indenter were not computed by Hertz in detail, but are calculable from equations derived by Huber [10]. The radius of the circle of contact between indenting sphere and flat specimen is given by

$$a^3 = \frac{K}{2G} P r, \quad (3)$$

where K is a dimensionless constant expressible in terms of the shear moduli G , G' , and Poisson's ratios ν , ν' of specimen and indenter materials respectively:

$$K = \frac{3}{4} \left\{ (1 - \nu) + (1 - \nu') \frac{G}{G'} \right\}. \tag{4}$$

By eliminating P from (2) and (3) we may write the indentation pressure as

$$p_0 = \left(\frac{2G}{\pi K} \right) \frac{a}{r}. \tag{5}$$

Equation (5) thus provides a rigorous theoretical justification for the functional form of the indentation stress-strain characteristic (1) within the elastic range.

The curve corresponding to (5) has been calculated by inserting $G = 3.7 \times 10^{11}$ dyn/cm² (LiF), $G' = 7.5 \times 10^{11}$ dyn/cm² (steel), $\nu = \nu' = 1/3$ (giving $K \approx 3/4$), and is plotted in Fig. 3 as the broken line. The experimental data appear to approach this line at low indentation pressures. It was difficult to confirm (5) any more accurately than this, because plastic flow occurred under steel indenters at even the lowest loads attainable, and in the case of nylon spheres, where elastic impressions *were* readily obtainable, the area of contact could not be measured sufficiently accurately (cf. Section 2.2).

3.2 Initial dislocation motion

This stage of deformation, corresponding to the point Y on Fig. 3, is the most amenable to a quantitative study. For the Hertzian analysis outlined above remains valid up to the point just prior to the onset of irreversible deformation, and may thus be applied to determine both the critical indentation yield pressure and the spatial location of initial dislocation motion within the inhomogeneous stress field.

We now invoke standard plasticity criteria to the Hertzian stress field at the initial yield point. For a plastically isotropic solid we might thus expect the onset of flow to occur at that point within the indented specimen which maximises the greatest principal shear stress (Tresca criterion). A contour plot of the great-

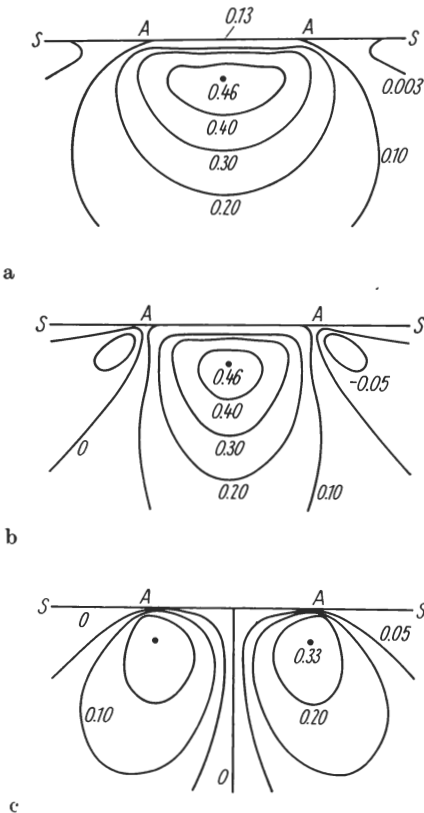


Fig. 5. Contours of shear stresses in a plane containing the axis of contact between sphere and flat specimen. (a) is for isotropic solid, (b) and (c) for crystal with (001) surface. AA represents diameter of contact, SS portion of the (infinite) surface. p_0 is the unit of stress. (a) Greatest principal shear stresses, contained in plane of symmetry; (b) shear stresses resolved on $\{110\}_{111}$ glide planes in direction of Burgers vector; plane of diagram either (010) or (100); (c) shear stresses resolved on $\{110\}_{100}$ glide planes in direction of Burgers vector; plane of diagram either (110) or (110)

test principal shear stresses under a spherical indenter (Fig. 5a) shows a maximum value of $0.46 p_0$ at a position located about $0.5 a$ below the surface along the axis of contact. (The case of flow initiation in isotropic materials under spherical indenters has been discussed in detail by Davies [11].) For a single crystal we have, in analogy with the Tresca criterion, the so-called critical resolved shear stress criterion, which requires maximisation of the shear stresses resolved along favourable glide planes in the slip direction. The shear stresses appropriately resolved for the $\{110\}_{45}$ and $\{110\}_{90}$ glide planes³⁾ are respectively shown in the contour maps of Figs. 5b and 5c: in these two plots the plane of the diagram contains both the axis of contact and the Burgers vector of the dislocations corresponding to the appropriate glide system. We see that the location and magnitude of the maximum resolved shear stress for the $\{110\}_{45}$ system is as for the isotropic case, while for the $\{110\}_{90}$ system the maximum shear stress has a value $0.33 p_0$ approximately $0.5 a$ directly below the circle of contact. The shear stresses do not attain high values at the crystal surface (the maximum possible shear stress attainable at the surface is calculated to be $0.16 p_0$). Thus on the basis of the critical resolved shear stress criterion one would favour dislocation initiation to occur on $\{110\}_{45}$ planes at a point about $0.5 a$ below the centre of contact; however, the maxima in Fig. 5 are by no means sharp, so that a reasonable variation in behaviour might well be anticipated.

Following the comprehensive studies by Gilman and Johnston [12] on dislocation mechanisms in LiF one is led to postulate that the dislocations nucleate heterogeneously in the form of loops and, on further increasing the indentation pressure beyond the yield point, that these loops subsequently expand outward from their sources to eventually intersect the crystal surface. The two essential features of this model (depicted schematically in Fig. 6), namely (i) that dislocation sources operate initially on $\{110\}_{45}$ planes, and (ii) that these sources are internal ones, are supported by an examination of indented LiF surfaces.

Fig. 7 shows a surface indented with a $1/2''$ nylon sphere and subsequently etched with the etchant "A" of Gilman and Johnston [6]. (In this and in all following micrographs the indented surface is designated as (001), and the edges of the diagram are along cube directions.) In order to distinguish between those dislocations grown-in and those freshly created during indentation the specimens were given a 30 s etch both before and after indentation: thus the grown-in dislocations, which remain immobile during indentation, are recognisable by their larger pit size. The orientation of the dislocation arrays in Fig. 7 is consistent

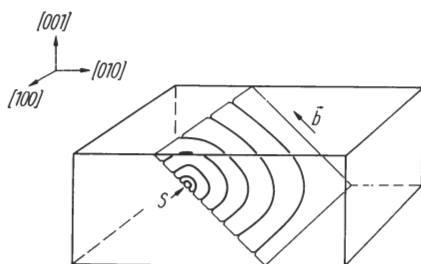


Fig. 6. Schematic representation of dislocation source operating at position of maximum resolved shear stress on a single $\{110\}_{45}$ glide plane within the Hertzian stress field. S denotes source, b , the direction of Burgers vector. (100) section shown intersecting S

³⁾ In crystals with the rocksalt structure dislocation glide occurs either on $\{110\}$ planes inclined at 45° to (001) (termed the $\{110\}_{45}$ planes) or inclined at 90° to (001) (termed the $\{110\}_{90}$ planes). The Burgers vectors lie along $\langle 110 \rangle$.

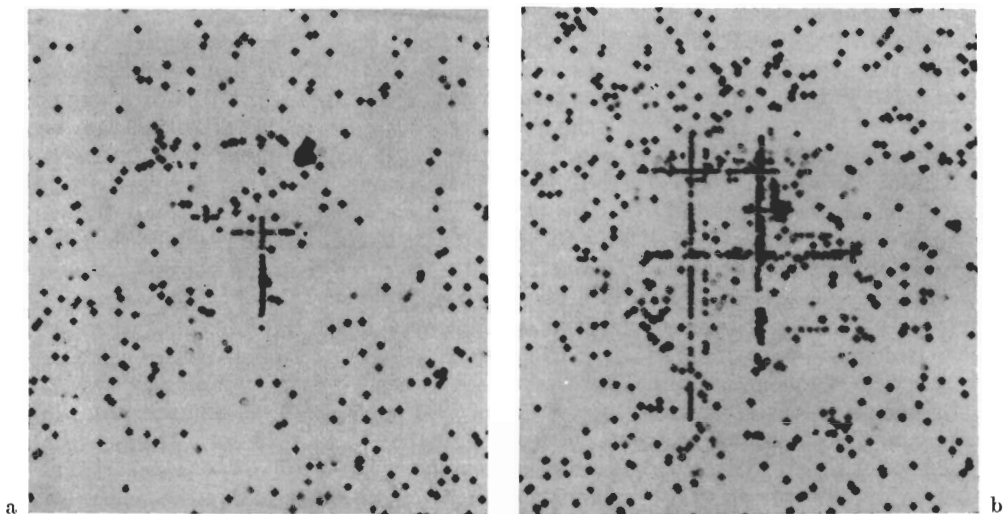


Fig. 7. Indentations made with $\frac{1}{2}$ " nylon ball on a (001) cleavage surface of LiF. Specimen etched before and after indentation. Indenter loads (a) 100, (b) 200 g. Width of field 500 μm

with slip on the $\{110\}_{45}$ planes, thus supporting the first of the two above features. At the lower loads one of the four possible sets of slip planes was usually found to be dominant, but as the load was increased the arrays tended to become more symmetrically disposed. No evidence of plastic flow could be determined for indenter loads much below 50 g. Transmission X-ray topographs [13] of similarly indented crystals (e.g. Fig. 8) confirm that 50 g represents an upper limit to the critical yield load for $\frac{1}{2}$ " nylon spheres.

The second essential feature of the dislocation model requires knowledge of the geometry of the dislocation arrays beneath the indented surface. This was

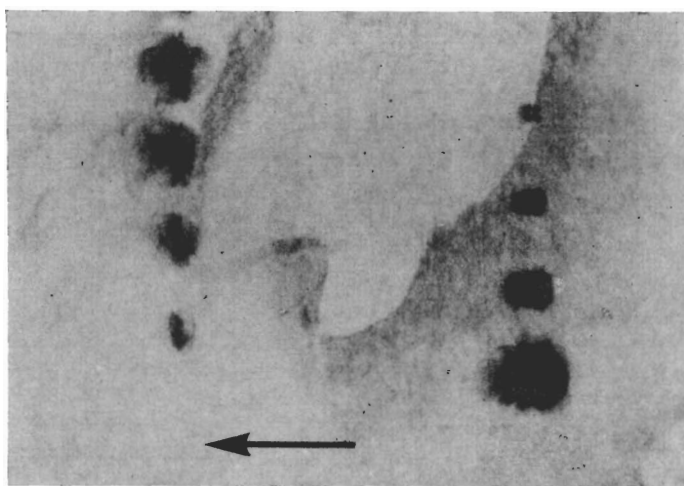


Fig. 8. Lang topograph of indented (001) cleavage surface of LiF. Radiation $\text{AgK}\alpha$, 020 reflection. Arrow, length 1 mm, denotes diffraction vector. Left-hand column made with $\frac{1}{2}$ " nylon ball, loads (top to bottom) 400, 300, 200, 100 g; right-hand column made with $\frac{1}{16}$ " steel ball, loads 25, 50, 100, 300 g

obtained by cleaving through the arrays, and then re-etching the crystal to reveal their intersection with the new cleavage plane (Fig. 9). The diagonal traces on the section planes in these figures clearly match the vertical traces of the (011) and (0 $\bar{1}1$) slip planes on the indented surface, while the horizontal traces likewise match the horizontal traces of the (101) and (10 $\bar{1}$) slip planes on the indented surface. The postulated depth, $0.5 a$, of the dislocation initiation point below the (001) surface is obtained by inserting $P_c = 50$ g (critical load), $r = 0.625$ cm, $G' = 0.1 \times 10^{11}$ dyn/cm² (manufacturer's specification for nylon, giving $K \approx 20$) into equation (3): the calculated depth of approximately $50 \mu\text{m}$ corresponds very closely to the points of mutual intersection of the traces of the (011) and (0 $\bar{1}1$) slip planes in the sectional view of Fig. 9. It is noted that the dislocation density generally tends to be greatest in this vicinity, as one would expect if sources were to operate there. The most conclusive evidence supporting the internal source postulate is obtained by comparing etch pit counts for the corresponding slip traces on the (001) and (100) surfaces. If surface sources were to be active each half-loop would intersect the (001) indentation surface at two points, and a subsequent favourably directed (100) cleavage plane (i.e. a plane intersecting *all* half-loops) at one point. It follows that, at best, the etch pit count for a particular slip trace on the (100) surface could equal half that for the matching trace on the (001) surface. For internal sources, on the other hand, similar considerations show that for a favourable (100) cleavage plane the corresponding factor could greatly exceed one half (e.g. in the hypothetical case in Fig. 6 the factor would be 11/6). Careful counts have revealed a number of cases in which the etch pit count factor exceeded one half⁴) (the (0 $\bar{1}1$) slip trace on the extreme right of the array in Fig. 9 providing a notable example). Thus the evidence points to the internal dislocation source as the agent for flow initiation on the $\{110\}_{45}$ planes in LiF, a mechanism which, in the absence of a detailed consideration of the Hertzian stress field, has not been specifically considered by other workers [6, 14, 15].

Having provided evidence to support the model in Fig. 6 we may now proceed to compute the critical stresses from the Hertzian theory. From Fig. 5b the critical resolved shear stress is

$$\tau_{0Y} \approx 0.46 p_{0Y}, \quad (6)$$

where p_{0Y} is the mean indentation pressure at the initiation point Y in Fig. 3. If σ_{0Y} is the corresponding compression stress at which dislocation motion begins in the compression test, then for crystals aligned along [001] the critical resolved shear stress on $\{110\}_{45}$ planes is

$$\tau_{0Y} \approx \sigma_{0Y}/2. \quad (7)$$

Combining (6) and (7) we have

$$p_{0Y} \approx \sigma_{0Y}. \quad (8)$$

Inserting into (5) the data for the nylon spheres for critical loading we obtain $p_{0Y} \approx 2$ kg/mm². This compares with $\sigma_{0Y} \approx 0.8$ kg/mm² corresponding to point Y in Fig. 4. Remembering that the quoted critical load in the indentation tests represents an upper limit, and bearing in mind that the non-ideal conditions existing in most compression specimens will act to reduce σ_{0Y} , these approximate

⁴) Of course, a factor of *less* than one half tells us nothing about the location of the source, this simply indicating that the sectioning cleavage has not intersected all the loops.

calculations indicate the ability of the ball indentation test to provide at least an upper limit to the initial yield stress of a plastic solid.

3.3 Growth of plastic zone to fracture

As the load on a spherical indenter is raised beyond the yield point the plastic zone grows in size. The theory of plasticity in its present state is unable to provide a formal solution of any problem where the elastic and plastic strains in crystals are comparable. We are therefore restricted to qualitative descriptions of the dislocation arrays as a function of increasing indentation pressure. Other

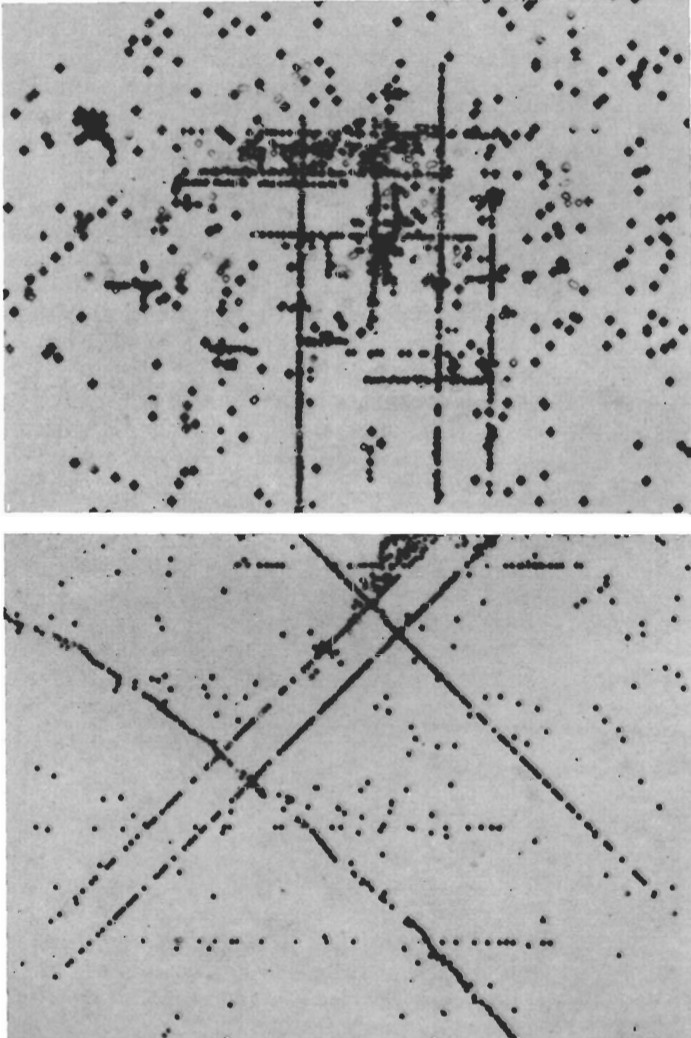


Fig. 9. (001) half-surface (top) and cleaved (100) cross-section (bottom) views of indent made on LiF with $\frac{1}{2}$ " nylon ball under 350 g load. Surface view shown after cleavage through indent. Width of field 500 μm . (The curved line of etch pits in the lower figure is a grain boundary)

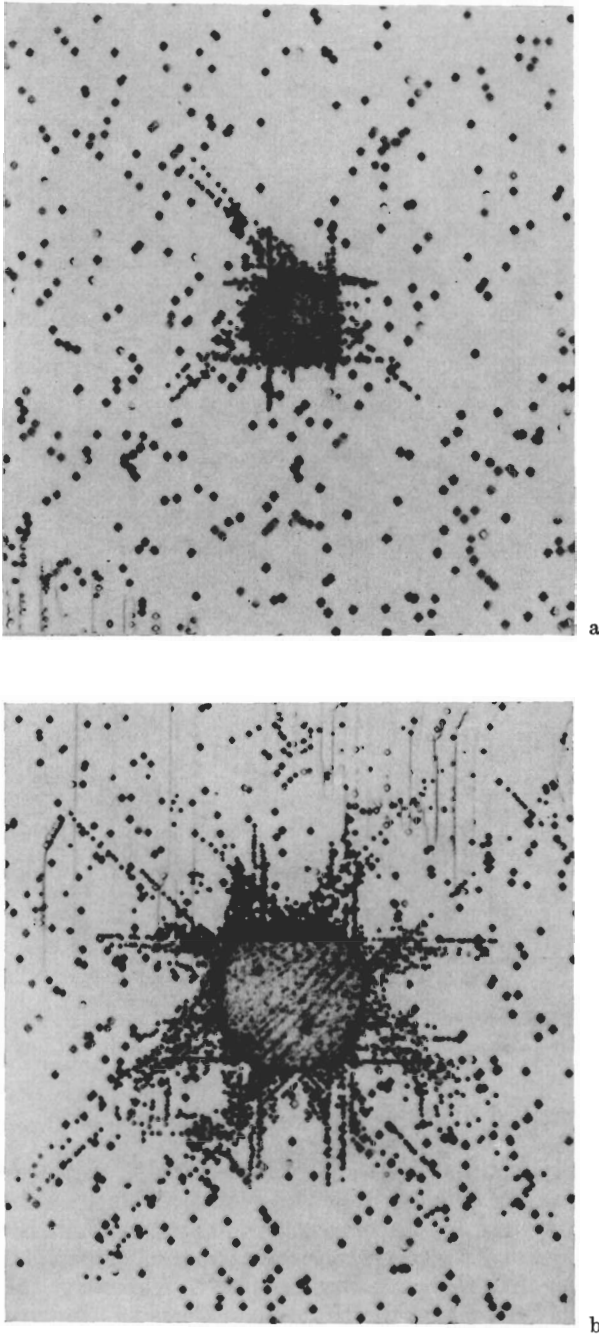


Fig. 10. Indentations made on (001) LiF surfaces with steel balls of $1/2''$ diameter at loads (a) 50, (b) 200 g. Surfaces etched before and after indentation. Width of field $500 \mu\text{m}$. (a) corresponds to $p_0 = 11 \text{ kg/mm}^2$, (b) to $p_0 = 16 \text{ kg/mm}^2$. The diagonal traces represent $\{100\}_{00}$ slip

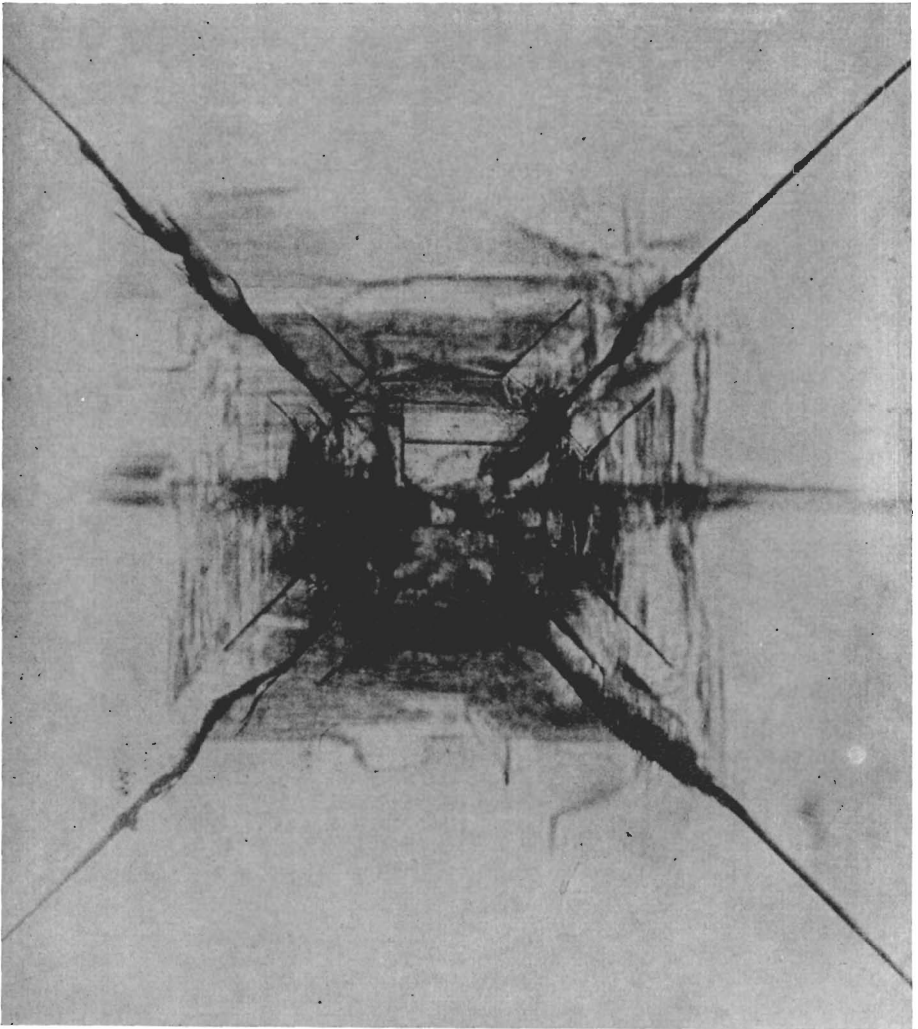


Fig. 11. Fracture pattern associated with an indentation on (001) LiF made with $1/16''$ steel ball at a load of 70 kg. Fracture viewed in transmitted light. Width of field 0.30 cm

workers have described similar patterns, but only for arbitrarily selected indentation loads [6, 9, 14 to 19].

Fig. 10 shows indentation patterns produced by $1/2''$ steel spheres at loads of 50 and 200 g. In Fig. 10a, corresponding to a point just above Y, it is evident that the $\{110\}_{90}$ system has become active. This we might have anticipated, since we saw in Section 3.2 that the shear stresses resolved for $\{110\}_{90}$ slip are not very much smaller than those resolved for $\{110\}_{45}$ slip. Once the initial slip has occurred on the $\{110\}_{45}$ planes the Hertzian analysis no longer remains valid, so that there is no means for making a quantitative estimate of the initiation point for $\{110\}_{90}$ slip. As the indentation pressure is raised toward point A on the stress-strain curve the activity of the $\{110\}_{90}$ system begins to increase at a great

ter rate than that of the $\{110\}_{45}$ system. In Fig. 10b, where the density of slip traces has increased but is still sparse, both systems appear to have a comparable activity, while at even higher loads, within the "plateau" region AB of Fig. 3, where the slip traces completely surround the impression, the $\{110\}_{90}$ "arms" of the dislocation array extend rapidly outward at the expense of the others. Thereafter, within the range BF of the stress-strain curve, the pattern remains much the same in its geometrical shape, although it grows rapidly in size, and takes on the appearance of rosettes obtained with pointed indenters. Ultimately, at F, the specimens tend to fracture (Fig. 11).

The slip behaviour described above differs significantly from that shown by uniaxially compressed specimens. For while the $\{110\}_{90}$ slip system plays an important role in the indentation tests this same system remains essentially passive throughout a compression test. Thus the indentation behaviour appears to be characterised by the gradually increasing assertion of the $\{110\}_{90}$ slip system over the competing $\{110\}_{45}$ system, while the compression behaviour appears to be determined rather by changes in the relative activity of the four planes within the $\{110\}_{45}$ system only. Also, the pressure in a ball indentation test needs to be increased by a factor of about 85 from that at yield to attain the "plateau" of the stress-strain curve (Fig. 3), while in the compression test the corresponding factor is only 1.5 (Fig. 4). Thus the indentation curve deviates comparatively slowly from elastic behaviour, this being attributable to the constraining effect of the surrounding, elastically distorted, crystal matrix on the expanding plastic zone localised just below the indenting sphere. Once the plastic zone completely surrounds the indenter contact area this constraining effect would appear to become minimised and a state of "full plasticity" is thereby achieved. The inevitable mutual interaction between slip on different planes as the deformation becomes more intense presumably accounts for the "work-hardening" region of the indentation stress-strain curve and for the complex fracture pattern that follows [17].

4. Conclusion

It was pointed out in the introduction that indentation testing is widely used as a means for indicating the hardness characteristics of a solid. The so-called hardness number H (indenter load/actual area of impression) is of practical use as an indicator of material hardness; for isotropic materials the hardness number is relatable to the yield stress σ_Y in a simple compression test⁵⁾ by means of the Tabor relation [3],

$$H \approx p_0 = c \sigma_Y, \quad (9)$$

c being a constant whose value is about 3. Equation (9) is largely empirical, but has received some theoretical justification for indentations in ideally rigid-plastic isotropic solids. Apart from the advantage of simplicity in measurement the Tabor relation has, indeed, been suggested as the only practical means of evaluating yield stresses for those harder solids which behave in a completely brittle manner in compression and other conventional testing arrangements. With a suitable choice of indenter geometry the fracture tendencies of a speci-

⁵⁾ σ_Y in this case representing the stress at which deviation from the linear elastic portion of the compression stress-strain curve first occurs.

men can hopefully be suppressed by the largely hydrostatic compressive stresses around the indenter, thus permitting a permanent impression to be made and a yield stress σ_Y to be evaluated [20]. This procedure relies on two factors: firstly that the impression is indeed a result of plastic flow, and secondly, that the constant c in (9) is specifiable and remains invariant for any experiment.

It must be emphasised that Tabor's relation is based upon the assumption of isotropic plasticity. Here we are concerned with single crystals, whose plastic behaviour is highly anisotropic. In this case we have no basis for pre-determining the factor c , which will become strongly dependent upon the orientation of the crystal with respect to the loading axis. For instance, in our experiments we have loaded LiF crystals along [001], for which we find $c \approx 50$ to 60 (compare p_0 and σ within the fully plastic region of Figs. 3 and 4). Westbrook [21] has made a similar observation for diamond pyramid indentations in numerous crystals with the rocksalt structure. Now if the crystals were aligned along [111] there would be zero component of shear stress on any of the $\{110\} \langle 110 \rangle$ slip systems in an ideal uniaxial compression test, while for a spherical indenter the inhomogeneous nature of the Hertzian stress field would ensure a finite component of shear stress on all glide planes: thus for this particular orientation yield would occur only in the indentation experiment and c would effectively be zero. Thus we expect c to vary over a wide range of values, particularly for LiF and the other rocksalt crystals which possess restricted glide systems. In metals the slip systems are more flexible [20] and less variation in c would be anticipated: in static ball tests on single crystals of lead, for instance, c varies only between 2.3 and 5 over a wide range of surface orientation [22]. Thus the Tabor relation can not be regarded as a reliable guide to the yield strength of single crystal specimens, despite its increasingly widespread use in the literature as such.

One might therefore, in an attempt to establish the concept of hardness on a firmer physical basis, alternatively advocate the use of the ball indentation yield pressure p_{0Y} as a measure of specimen hardness; the approach would have the advantage of relating the hardness of a material directly to a characteristic property of its deformation behaviour, namely (in the present case) the stress required to activate dislocation sources. This approach was actually proposed by Hertz [2] as long ago as 1882, but there has been little attempt to develop the idea since that time. There is, of course, the severe disadvantage in that comparatively sophisticated experimentation is required to establish the conditions of initial flow, as is evident from the present study on LiF, which makes the Hertzian concept of hardness impracticable as a means for routine hardness measurement. Nevertheless, it is evident that by developing techniques for detecting the *onset* of irreversible deformation within the Hertzian stress field the physical processes contributing to the general mechanical behaviour of a solid, and the variables affecting these processes, may be studied in a controlled and quantitative manner.

Acknowledgements

The authors wish to thank Mr. P. Holmes for his assistance in setting up the indenting equipment. They are also grateful to the School of Metallurgy (this University) and the Defence Standards Laboratories (Sydney) for making available their mechanical testing machines.

References

- [1] H. HERTZ, Hertz's Miscellaneous Papers, Chap. 5, Macmillan, London 1896.
- [2] H. HERTZ, Hertz's Miscellaneous Papers, Chap. 6, Macmillan, London 1896.
- [3] D. TABOR, The Hardness of Metals, Clarendon Press, Oxford 1951.
- [4] F. C. FRANK and B. R. LAWN, Proc. Roy. Soc. **A299**, 291 (1967).
- [5] E. W. SUCOV, J. Amer. Ceram. Soc. **45**, 575 (1962).
- [6] J. J. GILMAN and W. G. JOHNSTON, Dislocations and Mechanical Properties of Crystals, Eds. J. C. FISHER, W. G. JOHNSTON, R. THOMSON, T. VREELAND, Wiley, 1957 (p. 116).
- [7] J. J. GILMAN, J. appl. Phys. **30**, 1584 (1959).
- [8] R. W. DAVIDGE and P. L. PRATT, phys. stat. sol. **6**, 759 (1964).
- [9] E. VOTAVA, S. AMELINCKX, and W. DEKEYSER, Acta metall. **3**, 89 (1955).
- [10] M. T. HUBER, Ann. Phys. (Germany) **14**, 153 (1904).
- [11] R. M. DAVIES, Proc. Roy. Soc. **A197**, 416 (1949).
- [12] J. J. GILMAN and W. G. JOHNSTON, Solid State Phys. **13**, 147 (1962).
- [13] A. R. LANG, J. appl. Phys. **30**, 1748 (1959).
- [14] J. F. PETROFF and A. AUTHIER, phys. stat. sol. **13**, 373 (1966).
- [15] K. MEYER and E. GRAGERT, phys. stat. sol. **6**, 803 (1964).
- [16] K. MEYER and E. GRAGERT, phys. stat. sol. **3**, 2005 (1963).
- [17] E. GRAGERT and K. MEYER, phys. stat. sol. **9**, 33 (1965).
- [18] W. H. VAUGHAN and J. W. DAVISSON, Acta metall. **6**, 554 (1958).
- [19] A. S. KEH, J. appl. Phys. **31**, 1538 (1960).
- [20] A. KELLY, Strong Solids, Clarendon Press, Oxford 1966.
- [21] J. H. WESTBROOK, G. E. Research Report, No. 58-RL-2033, Schenectady, New York 1958.
- [22] T. D. DUDDERAR and J. DUFFY, Internat. J. Mech. Sci. **9**, 621 (1967).

(Received July 29, 1969)